INITIAL STEPS TOWARDS AUTOMATIC SEGMENTATION OF THE WIRE FRAME OF STENT GRAFTS IN CT DATA

A. Klein[1], W.K. Renema[2], L.J. Schultze Kool[2], C.H. Slump[1]

[1] Twente University, Signals and Systems group, The Netherlands
[2] Radboud University Nijmegen Medical Centre, The Netherlands

Abstract

For the purpose of obtaining a geometrical model of the wire frame of stent grafts, we propose three tracking methods to segment the stent's wire, and compare them in an experiment. A 2D test image was created by obtaining a projection of a 3D volume containing a stent. The image was modified to connect the parts of the stent's frame and thus create a single path. Ten versions of this image were obtained by adding different noise realizations. Each algorithm was started at the start of each of the ten images, after which the traveled paths were compared to the known correct path to determine the performance. Additionally, the algorithms were applied to 3D clinical data and visually inspected. The method based on the minimum cost path algorithm scored excellent in the experiment and showed good results on the 3D data. Future research will focus on establishing a geometrical model by determining the corner points and the crossings from the results of this method.

1 Introduction

Endovascular aortic replacement (EVAR) is an established technique, which uses stent grafts to treat aortic aneurysms in patients at risk of aneurysm rupture [2]. The long-term durability of these stent grafts is affected by the stresses and hemodynamic forces applied to them, and may be reflected by the movements of the stent graft itself during the cardiac cycle. Applying ECG-gated CTA [7, 11, 9] provides three dimensional datasets at different phases of the cardiac cycle, and thus provides insight in the stent's motion. These data can be used to calculate the forces caused by the hemodynamics [8]. However, this requires obtaining the geometric model of the stent's frame in the form of connected landmarks placed at corners and crossings.

In literature, several studies have been published on the segmentation of blood vessels. However, two-step approaches [13], which first segment the vessel using a vessel measure [6] followed by centerline extraction, are not suitable because of the gaps in the wire (caused by artifacts) and its sharp corners compared to blood vessels. Methods that fit spheres/ellipsoids to the vessel (e.g. [1]), and methods that segment the contour in slices perpendicular to the vessel centerline (e.g. [10]), will not work due to the small diameter of the wire (1 to 3 voxels) and its sharp corners. Region growing methods [3] have problems with leaks and gaps and need a second stage to find the geometry from the segmented voxels. Methods that use the minimum cost path method [5] are robust against gaps and artifacts (e.g. [4, 12]). However, these method cannot be applied in their default form since it requires the selection of a start point (and often an end point).

We propose three tracking algorithms that finds the optimal path along the stents' wire, and compare them in an experiment. The proposed methods are applicable to both 2D and 3D (anisotropic) data.

2 Methods

The basic assumption of the proposed methods is that once a position on the wire of the stent is known, a next position along the wire can be calculated with great confidence. Given a 3 dimensional image $V(\mathbf{x})$ with $\mathbf{x} = (x, y, z)$, the algorithm places multiple objects inside the volume, which we refer to as *walkers*. These walkers are initially positioned in a regular grid with a certain spacing in mm. Next, each walker moves to the voxel in its local environment that has the highest intensity, after which each walker will proceed autonomously through the data, while tracking the wire frame of the stent.

2.1 Method A: 1D growing

In each iteration, this method compares its second order neighbors (i.e. its 8 or 26 neighbors for 2D and 3D, respectively) and selects the neighbor with the highest intensity. If the intensity of the selected pixel/voxel is above a certain threshold, it will be the current position for the next iteration, otherwise the walker is discarded.

2.2 Method B: directional center of mass

The second proposed method uses a modified version of the center-of-mass (COM) method, in which the kernels are Gaussian smoothed and multiplied by a direction-dependent weighting kernel. The Gaussian smoothing is applied to suppress the influence of voxels further away from the kernel center, and the weighting kernel is applied to maintain motion in the direction of the previous step (figure 1). Since the smoothed COM kernel can be represented by Gaussian derivative kernels, this operator can be considered a gradient operator biased for a certain direction.

We describe the elements of the direction dependent weighting kernel as $w_{\mathbf{k}}$, with $\mathbf{k} = (k_x, k_y, k_z)$ the kernel coordinate relative to the center of the kernel. Given the direction of the previous step $\mathbf{d}$, the angle for each kernel element is $\alpha_{\mathbf{k}} = \arccos(\mathbf{k}/|\mathbf{k}| \cdot \mathbf{d}/|\mathbf{d}|)$. The weights of the kernel are calculated with:

$$w_{\mathbf{k}}(\alpha) = \cos(\alpha_{\mathbf{k}}) + 0.5. \quad (1)$$

Replacing $\alpha_{\mathbf{k}}$ gives:

$$w_{\mathbf{k}}(\mathbf{x}, \mathbf{d}) = \frac{\mathbf{x}}{|\mathbf{x}|} \cdot \frac{\mathbf{d}}{|\mathbf{d}|} + \mathbf{0.5}. \quad (2)$$

Each iteration, a patch of data p is sampled, centered around the current position. For each dimension, this patch is multiplied with the corresponding Gaussian derivative kernel and with the weighting kernel to yield the new (unnormalized) direction:

$$\mathbf{d}_{new} = \left(\sum_{\forall \mathbf{k}} p_{\mathbf{k}} g_{\mathbf{k},x} w_{\mathbf{k}}, \sum_{\forall \mathbf{k}} p_{\mathbf{k}} g_{\mathbf{k},y} w_{\mathbf{k}}, \sum_{\forall \mathbf{k}} p_{\mathbf{k}} g_{\mathbf{k},z} w_{\mathbf{k}} \right), \quad (3)$$

where $g_{\mathbf{k},x}$, $g_{\mathbf{k},y}$ and $g_{\mathbf{k},z}$ represent the Gaussian derivative kernels for the x, y and z direction, respectively. Next, $\mathbf{d}_{new}$ is combined with the old value of $\mathbf{d}$ such that the angle between the old and the new direction is limited by a predefined value. This angle threshold gives control over the walkers' affinity to proceed in the same direction, and thus prevents the walker from "making a u-turn".

The new position is determined by selecting the voxels which are in the found direction, and choosing the one with the highest intensity.

2.3 Method C: minimum cost path

The third proposed algorithm is based on the minimum cost path algorithm [5, 12], which is applied in a step-by-step tracking approach. Given the speed (representing the inverse cost function) in each voxel $s_{\mathbf{x}}$, the
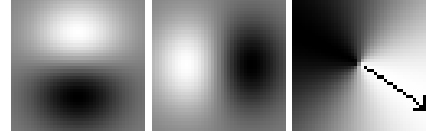

Figure 1: Illustration of the two 2D smoothed COM kernels and the direction-dependent weighting kernel.

Algorithm 1 The minimum cost path algorithm

```
01 init the time map tx = ∞ ∀x
02 init the frozen map fx = 0 ∀x
03 init tx = 0 for the start nodes
04 insert the start nodes in list L
05 while not isempty(L):
06    take node m from L with min.   tm
07    set fm = 1
08    for n in neighborsOf(m):
09       if fn == 0:
11          d = euclidianDist(n,m)
12          t = tm + d/sn
13          if t < tn:
14             tn = t
15             dn = dm + d
16             if n not in L:
17                insert n in L
```

---

algorithm iteratively calculates the time $t_{\mathbf{x}}$ it takes to travel from the start node to any other node in the image (see algorithm 1). The fastest (minimum cost) path can be found to any point $\mathbf{x}$ by backtracking in the resulting time map.

We modified the algorithm such that it stops as soon as a distance $d_{\mathbf{x}}$ larger than d_{min} is encountered (figure 2). Since the algorithm selects the node with the minimum cumulative cost ($t_{\mathbf{x}}$) at each iteration, the first node $\mathbf{x}$ for which $d_{\mathbf{x}} > d_{min}$ is the node that is "traveled easiest to", and therefore has the highest probability of being positioned on the same wire as the previous node.

To be robust against artifacts, only the first half of the path from the start node to $\mathbf{x}$ is used. This path is appended to the total walked path and its last node will
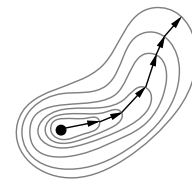

Figure 2: Illustration of the proposed minimum cost path approach. The front (the voxels in L) moves outward until the cumulative distance of the path is larger than d_{min}.
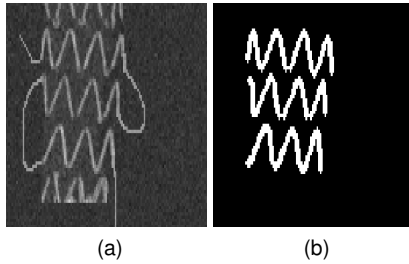
Figure 3: Illustration of the 2D test image (a) and the used mask to calculate performance(b).

be the start node for the next iteration. At the start of the next iteration the last 20 nodes in the total walked path are set frozen to prevent backtracking.

The speed $s_{\mathbf{x}}$ is calculated with:

$$s_{\mathbf{x}} = 2^{V(\mathbf{x})/\delta}, \qquad (4)$$

where δ is a scalar number. Using this speed map has the effect that the path through a single voxel with a CT-value of a, is equally fast as another path through two voxels with CT-values of $a + \delta$. In other words, the optimal path has a strong affinity for high intensity voxels, rather than taking the shortest route. This prevents the algorithm to cut the sharp corners present in our data. In our method we used a value of $\delta = 100$.

3 Experiments

A 2D test image (figure 3a) was created by obtaining a projection of a 3D volume containing a stent. The image was modified to connect the three parts of the stents' frame and thus create a single path. Ten versions of this image were obtained by adding different noise realizations (Gaussian noise with a standard deviation of 75 CT-values). A walker was placed to walk down the path of the ten images, after which the traveled paths were compared to the known correct path (figure 1b) to determine the performance of each method. Beforehand, the same setup was used (but with different noise realizations as in the experiment) to choice the optimal parameters for each method.

Additionally, the algorithms were applied to 3D clinical data using multiple walkers, and the result was visually inspected.

4 Results and Discussion

From the average correspondence of the walked paths with the correct path (table 1) it can be seen that the method A performed poorly, while method C performed

Method:	A	B	C
Performance:	0.32	0.88	1.00

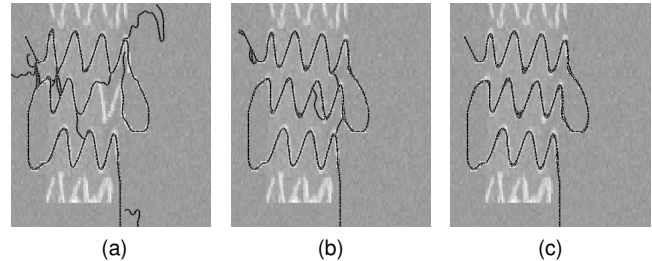Table 1: The quantitative results of the experiments.

Figure 4: Illustration of the walked paths of the three methods for the 10 noise realizations.

excellent. The traveled paths for each method (figure 4) confirm these findings. Visual inspection of the method applied to 3D data (figure 5) shows the same trend.

During the process of the experiments, it was found that the performance of method B is sensitive to the chosen parameters (such as the scale of the kernels and the angle limit). In contrast, method C was very robust for the choice of its parameter values (d_{min} and δ).

We note that method C can be seen as a generalization of method A; instead of selecting the next position from the direct neighbors, the most probable voxel at a certain distance from the current position is selected. The concept of incorporating a larger neighborhood in determining the most probable next position is also used in method B. However, method B is sensitive for nearby structures (e.g. other wires) and has problems with sharp corners.

In the current method, the walkers are unaware of each other. By connecting the walked paths when two walkers meet, the walkers should be able to work together to perform the segmentation task.

5 Conclusions and Future Work

We have described and compared three methods to track the wire frame of the stent graft in 3D CT data and 2D projections thereof. The best performing method is based on the minimum cost path method and is capable of obtaining near-perfect segmentation of the stent. The method is robust to unforeseen situations and variation in its parameters.

Future research will focus on establishing a geometrical model by determining the corner points and the
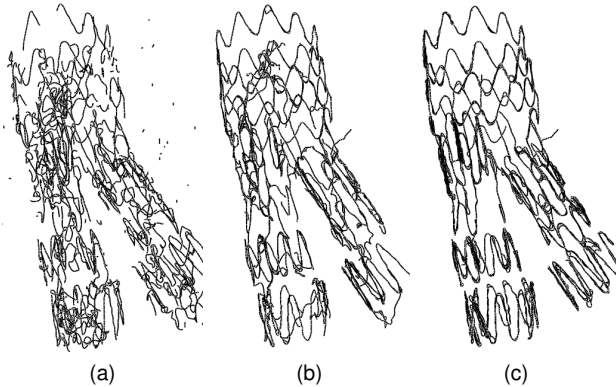
(a) (b) (c)

Figure 5: Illustration of the found paths of multiple walkers in a 3D volume.

crossings from the results of the proposed method.

6 References

[1] Thomas Beck, Christina Biermann, Dominik Fritz, Rudiger Dillmann, Josien P. W. Pluim, and Benoit M. Dawant. Robust model-based centerline extraction of vessels in CTA data. In *Medical Imaging 2009: Image Processing*, volume 7259, pages 72593O–9, Lake Buena Vista, FL, USA, February 2009. SPIE.

[2] Jan D. Blankensteijn, Sjors E.C.A. de Jong, Monique Prinssen, Arie C. van der Ham, Jaap Buth, Steven M.M. van Sterkenburg, Hence J.M. Verhagen, Erik Buskens, Diederick E. Grobbee, and the Dutch Randomized Endovascular Aneurysm Management (DREAM) Trial Group. Two-Year outcomes after conventional or endovascular repair of abdominal aortic aneurysms. *N Engl J Med*, 352(23):2398–2405, June 2005.

[3] Susanne Bock, Caroline Kuhhnel, Tobias Boskamp, and Heinz-Otto Peitgen. Robust vessel segmentation. volume 6915, page 114, April 2008.

[4] Thomas Deschamps and Laurent D Cohen. Fast extraction of minimal paths in 3D images and applications to virtual endoscopy. *MEDICAL IMAGE ANALYSIS*, 5:281—299, 2000.

[5] E.W. Dijkstra. A note on two problems in connexion with graphs. *Numerische Mathematik*, 1:269—271, 1959.

[6] Alejandro F Frangi, Wiro J Niessen, Koen L Vincken, and Max A Viergever. Multiscale vessel enhancement filtering. *Lecture Notes in Computer Science*, 1496:130—137, 1998.

[7] T. O. Fuchs, M. Kachelriess, and W. A. Kalender. System performance of multislice spiral computed tomography. *IEEE Engineering in Medicine and Biology*, 19:63—70, 2000.

[8] Almar Klein, Luuk J. Oostveen, Marcel J. W. Greuter, Yvonne Hoogeveen, Leo J. Schultze Kool, Cornelis H. Slump, and W. Klaas Jan Renema. Detectability of motions in AAA with ECG-gated CTA: a quantitative study. *Medical Physics*, 36(10):4616–4624, October 2009.

[9] Almar Klein, W. KlaasJan Renema, Luuk J. Oostveen, Leo J. Schultze Kool, and Cornelis H. Slump. A segmentation method for stentgrafts in the abdominal aorta from ECG-gated CTA data. In *Proceedings of SPIE*, pages 69160R–69160R–10, San Diego, CA, USA, 2008.

[10] Jack Lee, Patricia Beighley, Erik Ritman, and Nicolas Smith. Automatic segmentation of 3D micro-CT coronary vascular images. *Medical Image Analysis*, 11:630—647, 2007.

[11] Bart E. Muhs, K. L. Vincken, J. van Prehn, M. K. Stone, L. W. Bartels, M. Prokop, F. L. Moll, and H. J. Verhagen. Dynamic Cine-CT angiography for the evaluation of the thoracic aorta; insight in dynamic changes with implications for thoracic endograft treatment. *European journal of vascular & endovascular surgery*, 32(5):532—536, 2006.

[12] Onno Wink, Alejandro F Frangi, Bert Verdonck, Max A Viergever, and Wiro J Niessen. 3D MRA coronary axis determination using a minimum cost path approach. *Magnetic Resonance in Medicine: Official Journal of the Society of Magnetic Resonance in Medicine / Society of Magnetic Resonance in Medicine*, 47(6):1169–1175, June 2002. PMID: 12111963.

[13] Stefan Worz, William J. Godinez, Karl Rohr, Josien P. W. Pluim, and Benoit M. Dawant. Segmentation of 3D tubular structures based on 3D intensity models and particle filter tracking. In *Medical Imaging 2009: Image Processing*, volume 7259, pages 72591P–8, Lake Buena Vista, FL, USA, February 2009. SPIE.